INTERNATIONAL JOURNAL OF PRECISION ENGINEERING AND MANUFACTURING Vol. 16, No. 12, pp. 2537-2543 NOVEMBER 2015 / 2537
DOI: 10.1007/s12541-015-0325-5 ISSN 2234-7593 (Print) / ISSN 2005-4602 (Online)

A Mechanism for a Deployable Optical Structure of a Small Satellite

Junwoo Choi[1], Dongkyu Lee[1], Kukha Hwang[1], and Byungkyu Kim[1,#]

1 School of Aerospace and Mechanical Engineering, Korea Aerospace University, 76, Hanggongdaehak-ro, Deogyang-gu, Goyang-si, Gyeonggi-do, 10540, South Korea
Corresponding Author / E-mail: bkim@kau.ac.kr, TEL: +82-2-300-0101, FAX: +82-2-3158-2191

KEYWORDS: Deploying mechanism, Deployable optical structure, Joint clearance, Alignment error, Passive-deploying

In this paper, we present a deployment mechanism that is applicable to a deployable optical structure where the focus is on satellite miniaturization. It is designed with a passive deployment mechanism that utilizes a spring hinge. In order to confirm the feasibility of the designed deployable mechanism, we theoretically analyze the alignment errors (de-space, tilt, and de-center) that influence the optical performance of the structure. The theoretical results are as follows: a de-space of 180.0 μm, a tilt of 1941.3 μrad, and a de-center of 45.3 μm. In addition, we measure alignment errors to evaluate the actual alignment errors for a manufactured deployable mechanism. The experimental results are as follows: a de-space of 180.2 μm, a tilt of 218.8 μrad, and a de-center of 617.5 μm. Finally, we investigate the factors causing the differences between the theoretical and experimental values, and we suggest a method for improving the alignment errors.

Manuscript received: January 13, 2015 / Revised: August 19, 2015 / Accepted: October 10, 2015

NOMENCLATURE

L = length of panel
h = height of deployment mechanism
r = magnitude of joint clearance
sh = magnitude of hole margin for the screw assembly
sr = tightened degree of screw
θ = rotation between global coordinate system and local coordinate system
$\overrightarrow{cl_j}$ = error vector due to joint clearance
$\overrightarrow{cl_{sh}}$ = maximum error vector when fastening spring hinge and hole
$\overrightarrow{cl_{sr}}$ = error vector by degree of tightening of screw
$\overrightarrow{cl_j}(i)$ = error vector due to joint clearance of i-th case
$\overrightarrow{cl_j}(j)$ = error vector due to joint clearance of j-th case
$\overrightarrow{cl_{sh}}(k)$ = error vector when fastening spring hinge and hole of k-th case
$\overrightarrow{cl_{sr}}(l)$ = error vector by degree of tightening of screw of l-th case
$\overrightarrow{cl}$ = error vector in a,b,c,d that are considered an error of all kinds
X = x component of global coordinate
Y = y component of global coordinate
Z = z component of global coordinate
x = x component of local coordinate
y = y component of local coordinate
z = z component of local coordinate
$\overrightarrow{a_{ideal}}$ = ideal position vector of $\vec{a}$
$\overrightarrow{b_{ideal}}$ = ideal position vector of $\vec{b}$
$\overrightarrow{c_{ideal}}$ = ideal position vector of $\vec{c}$
$\overrightarrow{d_{ideal}}$ = ideal position vector of $\vec{d}$
$\overrightarrow{a_{real}}$ = real position vector of $\vec{a}$
$\overrightarrow{b_{real}}$ = real position vector of $\vec{b}$

$\overrightarrow{c_{real}}$ = real position vector of $\vec{c}$

$\overrightarrow{d_{real}}$ = real position vector of $\vec{d}$

$\vec{a_i}$ = i-th case of real position vector of $\vec{a}$

$\vec{b_j}$ = j-th case of real position vector of $\vec{b}$

$\vec{c_k}$ = k-th case of real position vector of $\vec{c}$

$\vec{d_l}$ = l-th case of real position vector of $\vec{d}$

$\vec{v_1} = \vec{a_i} - \vec{b_j}$

$\vec{v_2} = \vec{b_j} - \vec{c_k}$

1. Introduction

Since the 1990s, under the slogan "Faster, Better, Cheaper, Smaller," research efforts on satellite miniaturization have been actively conducted with the purpose of cost reduction.[1] In a conventional satellite, the optical structure requires a lot of space through which light passes because it needs the focal distance to obtain an image. In the case of GeoEye-1, launched in 2008, the height of the optical structure occupies two thirds of the total height of the satellite.[2] In order to miniaturize a satellite, it is essential to decrease the volume required by the optical structure. Therefore, optical structures employing various deployable mechanisms are currently being researched in order to decrease the volume of the optical structure. A typical example is NASA's Nuclear Spectroscopic Telescope Array (NuSTAR). In particular, NuSTAR was able to successfully secure about a 10-m focal distance via its Able Deployable Articulated Mast (ADAM) with an X-ray based telescope. Thus far, NuSTAR is the only deployable optical structure that utilizes a mast to have been developed. Its expandability and versatility are excellent due to its modular mast.[3] In addition, three other programs - the Beijing University of Aeronautics and Astronautics Satellite (BUAA-Sat),[4] Dobson Space Telescope (DST)[5] of the Technical University of Berlin, and Pico-satellite for Remote-sensing and Innovative Space Missions (PRISM) of the University of Tokyo - have reported on applying a deployable mechanism to the optical structure of their satellites.[6] NuSTAR and BuAA-Sat both achieved high deployment ratios with complex structures. On the contrary, DST has a simple structure with a low deployment ratio. Although PRISM, with its high deployment ratio, was successfully launched and loaded on an aimed orbit, it showed a very coarse ground resolution of 30 m due to the instability of the structure.

In the proposed mechanism, we consider three key design points - the simple structure, a high deployment ratio (~4), and deployment without any additional actuators. In addition, we set up the requirement of the alignment specifications between primary and secondary mirrors that are able to supply a 1-m ground resolution. Then, a deployable mechanism to satisfy the above requirements is designed for an optical structure. Based on the concept design, we theoretically investigate alignment errors that might be generated from assembly errors originating from joint clearance and component fabrication. Finally, the alignment errors are measured after fabricating the deployable structure.

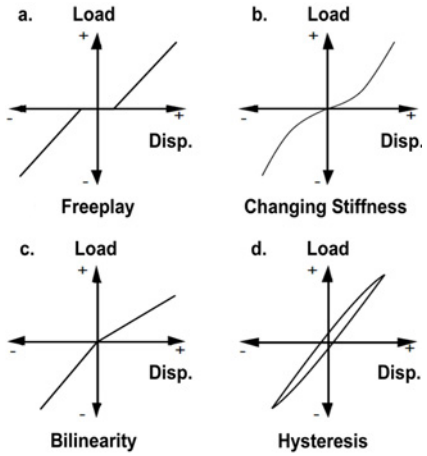

Fig. 1 Nonlinear behavior of mechanical joints[7]

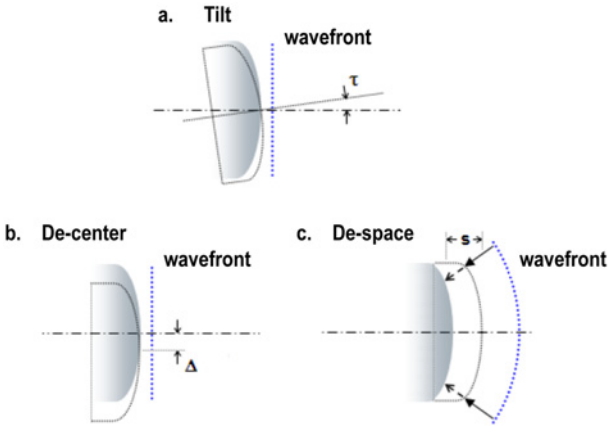

Fig. 2 Definition of tilt, de-center and de-space for mirrors[8,9]

2. Working Principles and Alignment Analysis

2.1 Alignment specifications

The deployment mechanism generally works based on the relative motion of the mechanism components. Thus, appropriate joint clearance should exist for the relative motion. This joint clearance results in the nonlinear behavior of components, as presented in Fig. 1. Alignment errors between the primary and secondary mirrors before and after deployment result from nonlinear behaviors and machining tolerances. The alignment errors are classified into tilt, de-center, and de-space in Fig. 2. Tilt is the degree to which the secondary mirror leans against the reference axis. De-center is the distance between the ideal and actual secondary mirror's central axis. De-space is the distance difference between the primary and secondary mirrors. The mechanism is designed to have a 1-m ground resolution when it is applied to the deployable optical structure. To set up the specifications of the mechanism alignment, we referred to the tilt, de-center, and de-space requisites of the multifunctional satellite,-KOMOSAT-3, which supplies a 1-m ground resolution with a fixed-type optical structure.[2] The required alignment specifications are shown in Table 1. The primary purpose of developing a deployable optical structure is to save inner

Table 1 Required alignment specifications

Classification	Optical alignment error
De-space	10 μm
De-center	10 μm
Tilt	100 μrad

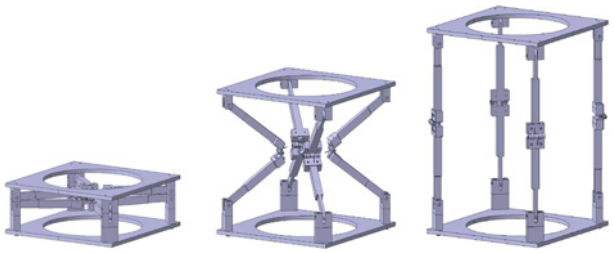

Fig. 3 Proposed deploying mechanism

space within the nose fairing by loading a deployable optical structure in a stowed state when the satellite is launched.

Hence, the deployment ratio of the structure, the difference between the stowed height and deployed height, is an important parameter. Referring to the deployment ratio of DST from the Technical University of Berlin, we determined the size and deployment ratio needed to achieve the design requirements necessary for 1-m ground resolution - a stowed height of 67 mm, a deployed height of 263 mm, and a deployment ratio of 3.93. The prototype was manufactured at a 1/3 scale for a feasibility test.

2.2 Working principles

As shown in Fig. 3, the proposed mechanism consists of eight linkages, eight joints, four spring hinges, and two panels, on which the primary and secondary mirrors will be installed. Until the launching vehicle reaches the target orbit, the proposed mechanism will remain in a stowed state. Once it arrives, the proposed mechanism will be deployed by the passive mechanism activated by the restoring force of the spring hinge without any additional actuator. Overall, the mechanism is designed to be comprised of simple structures so as to minimize the volume of the optical structure.

2.3 Theoretical alignment errors analysis

Alignment errors significantly influence the optical performance of the optical structure. Therefore, the alignment errors need to be analyzed theoretically before manufacturing the proposed mechanism. In order to analyze the alignment errors (de-center, de-space and tilt) of the proposed mechanism, it is necessary to investigate the position for each joint of each supporting modules.[10] Then, we can obtain the real position of the upper plate joint by adding its ideal position, which is set up in the design stage, to the cumulated position errors from the lower panel joint to the upper panel joint in one supporting module. The causes of position errors can be classified into errors due to joint clearance, errors due to the hole margin for the screw assembly, and errors due to the screw tightening degree. Errors due to joint clearance can be changed according to the rotation of the joint in the link since connected components by the joint have fabrication tolerance. Errors

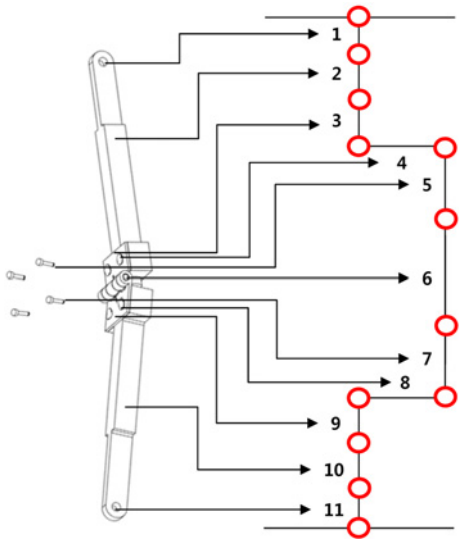

Fig. 4 Error type and error location in one supporting module of the deployment mechanism[11]

Table 2 Type and place of error occurrence

Part number	Description
1	Error due to joint clearance
2	Linkage
3	Spring hinge
4	Error due to hole margin for the screw assembly
5	Error due to screw tightening degree
6	Torsional spring
7	Error due to screw tightening degree
8	Error due to hole margin for the screw assembly
9	Spring hinge
10	Linkage
11	Error due to joint clearance

due to the hole margin for the screw assembly during deployment are generated within the range of the gap between the hole in the spring hinge and screw. Finally, errors due to the screw tightening degree are determined according to changes in the tightening condition of the screw after deployment.

The positions and types of the aforementioned potential three errors are presented in Fig. 4 and described in Table 2. Based on the classification in Fig. 4, the position error in each assembled component is independently calculated, and finally, the cumulated position errors from the lower panel joint to the upper panel joint in one supporting module is obtained by adding the errors in sequence.

Fig. 5 shows the local and global coordinate systems that are used to analyze the theoretical alignment errors. Additionally, Fig. 6 shows the configuration of the position vector, which is used in the theoretical alignment error analysis.

The z-axis direction of the local coordinate system at the center of the joint hole is equal to the z-axis direction of the global coordinate system, and the y-axis direction is equal to the rotation axis direction of the joint hole. The origin of the global coordinate and the origin of the local coordinate are positioned at the center of the lower panel and the center of the joint hole, respectively.

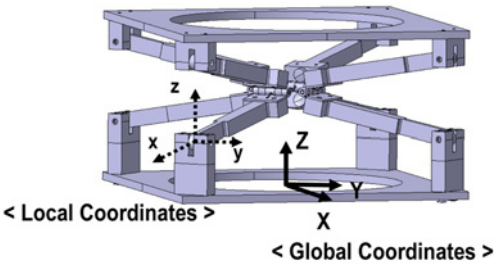

Fig. 5 Coordinate systems on the mechanism

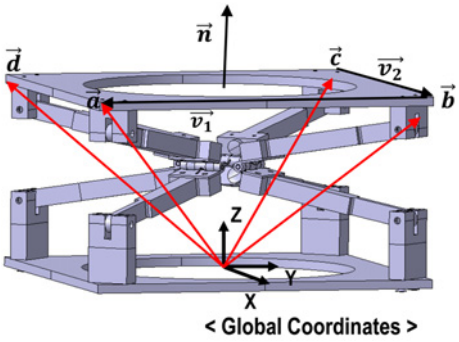

Fig. 6 Position vector used in analysis

For the theoretical analysis of the alignment error, we assumed the following:

- When deployment is completed, the linkage is upright at 90°
- Joint clearance occurs toward the x- and z-axis of the local coordinate system.
- Errors due to the hole margin for the screw assembly used to install the spring hinge occur toward the z-axis.
- Errors due to the screw tightening degree of a screw for the spring hinge occur toward the x-axis.
- The stiffness of the spring does not change.
- The machined parts are rigid.

In the event that the maximum joint clearance resulting from machining tolerance is *r*, the two linkages connected by a pin in the joint have an error of up to *2r*, as shown in Fig. 7. Accordingly, the size of the error vector generated at each joint is *2r*. Therefore, the position error vectors of a joint clearance based on the local coordinate system can be presented as follows:

$$\overrightarrow{cl_{j1}} = [+2r, 0, 0] \quad \overrightarrow{cl_{j2}} = [-2r, 0, 0]$$
$$\overrightarrow{cl_{j3}} = [0, 0, +2r] \quad \overrightarrow{cl_{j4}} = [0, 0, -2r] \tag{1}$$

When the spring hinge is combined with the linkage, the center of the spring hinge hole may not match exactly with the center of the screw. It corresponds to assembly errors that occurred during parts assembly. Accordingly, the error due to the hole margin for the screw assembly occurs toward the z-axis direction, as shown in Fig. 8. The maximum size of the error in the screw assembly (*sh*) can be [0, 0, +*sh*] or [0, 0, -*sh*]. After two errors are extracted by a duplicate combination, superposing them, we can obtain the error vector relative to the local

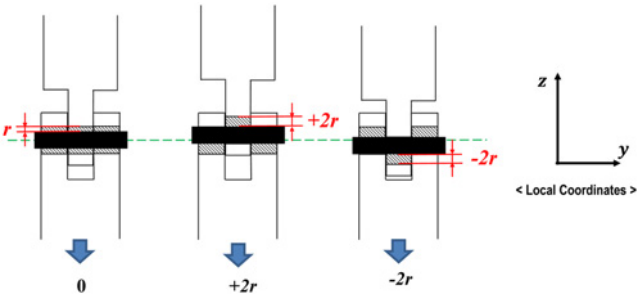

Fig. 7 Possible clearance due to the z-axis direction of the joint clearance[12]

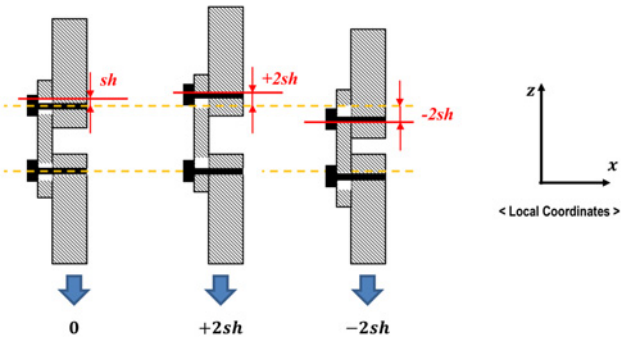

Fig. 8 Error due to the hole margin for the screw assembly

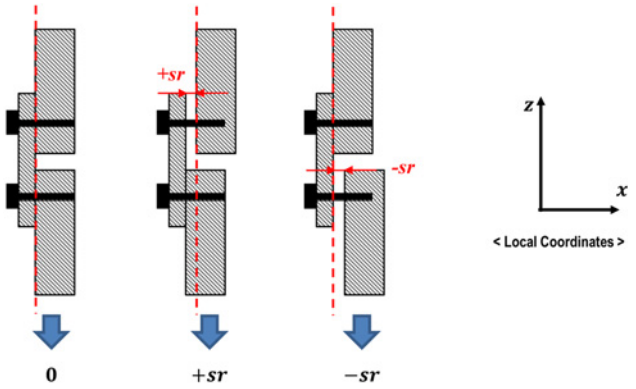

Fig. 9 Error due to the screw tightening degree

coordinate system as follows:

$$\overrightarrow{cl_{sh1}} = [0, 0, +2sh] \quad \overrightarrow{cl_{sh2}} = [0, 0, 0] \quad \overrightarrow{cl_{sh3}} = [0, 0, -2sh] \tag{2}$$

When we assemble the spring hinge and linkage using the screw, a screw can be excessively tightened (-*sr*) or under-tightened (+*sr*) compared to a designed position. Based on Fig. 9, the position error vectors for the local coordinate system can be presented as follows:

$$\overrightarrow{cl_{sr1}} = [+sr, 0, 0] \quad \overrightarrow{cl_{sr2}} = [0, 0, 0] \quad \overrightarrow{cl_{sr3}} = [-sr, 0, 0] \tag{3}$$

One supporting module consists of a lower panel joint hole and

linkage, a linkage and spring hinge, a spring hinge and a screw, a screw and a linkage, and a linkage and an upper panel joint hole. In one supporting module, hence, position error vectors generate at the joint holes of the upper/lower panels ($\vec{cl_j}(i)$ / $\vec{cl_j}(j)$) and at the spring hinge holes for the screw assembly ($\vec{cl_{sh}}(k)$ / $\vec{cl_{sr}}(l)$), respectively. Consequently, the total error vector ($\vec{cl}$), which occurs in one supporting module, can be formulated as follows:

$$\vec{cl} = \vec{cl_j}(i) + \vec{cl_j}(j) + \vec{cl_{sh}}(k) + \vec{cl_{sr}}(l) \tag{4}$$

The numbers of error vector cases with respect to the upper panel joint clearance, the lower panel joint clearance, the hole margin for the screw assembly, and the screw tightening degree are 4, 4, 3, and 3, respectively. As a result, the number of cases in terms of error vectors ($\vec{cl}$) is 144 from the calculated results of the aforementioned factors.

Since the degree of alignment is defined on the basis of the global coordinate, the error vector ($\vec{cl}$) relative to the local coordinate is converted to the vector ($\vec{cl_{global}}$) relative to the global coordinate as follows:

$$\vec{cl_{global}} = \begin{bmatrix} cos\theta & -sin\theta & 0 \\ sin\theta & cos\theta & 0 \\ 0 & 0 & 1 \end{bmatrix} \vec{cl} \tag{5}$$

Ideal position vectors ($\vec{a_{ideal}}$, $\vec{b_{ideal}}$, $\vec{c_{ideal}}$ and $\vec{d_{ideal}}$) from the origin of the global coordinate to each joint of the upper panel are presented as follows:

$$\begin{aligned} \vec{a_{ideal}} &= [+L/2 \quad -L/2 \quad h] & \vec{b_{ideal}} &= [+L/2 \quad +L/2 \quad h] \\ \vec{c_{ideal}} &= [-L/2 \quad +L/2 \quad h] & \vec{d_{ideal}} &= [-L/2 \quad -L/2 \quad h] \end{aligned} \tag{6}$$

The actual position vector from the origin of the global coordinate to each joint of the upper panel is obtained by adding the ideal position vector to the error vector, as shown in Fig. 10.

$$\begin{aligned} \vec{a_{real}} &= \vec{a_{ideal}} + \vec{cl_{global}} & \vec{b_{real}} &= \vec{b_{ideal}} + \vec{cl_{global}} \\ \vec{c_{real}} &= \vec{c_{ideal}} + \vec{cl_{global}} & \vec{d_{real}} &= \vec{d_{ideal}} + \vec{cl_{global}} \end{aligned} \tag{7}$$

However, some cases of calculated position vector cases do not satisfy the assumption of a rigid body for upper panel. Based on Eqs. 8 and 9 below, those values were excluded in the calculation process for the alignment error.

The upper panel has four joints to connect with each supporting modules. Thus, the distance between the two actual position vectors ($\vec{a_i}$, $\vec{b_j}$, $\vec{c_k}$ and $\vec{d_l}$) will be changed within the joint clearance range even though the upper panel is assumed to be a rigid body.

$$\begin{aligned} \left|\vec{a_i} - \vec{b_j}\right| &\le L + \sqrt{2}r & \left|\vec{b_j} - \vec{c_k}\right| &\le L + \sqrt{2}r \\ \left|\vec{c_k} - \vec{d_l}\right| &\le L + \sqrt{2}r & \left|\vec{d_l} - \vec{a_i}\right| &\le L + \sqrt{2}r \end{aligned} \tag{8}$$

If we have position vectors for three points, a plane in three-dimensional space can be obtained. In other words, one position vector is dependently determined by three position vectors for a rigid rectangular panel. As a result, the summation of the diagonally positioned vectors ($\vec{a_i}$ and $\vec{c_k}$, $\vec{b_j}$ and $\vec{d_l}$) should be the same. However, the upper panel has four joints, which each have clearance (r)

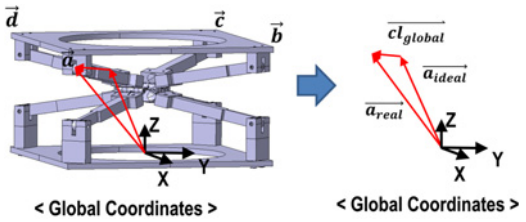

Fig. 10 Real position vector of a joint with the ideal position vector

Table 3 Theoretical alignment

Tolerance (μm)	De-space (μm)	Tilt (μrad)	De-center (μm)
40	180.0	1941.3	45.3

in the z-axis direction. Therefore, the difference between summations of the diagonally positioned vectors cannot be over $2r$.

$$\left|a_z + c_z - b_z - d_z\right| \le 2r \tag{9}$$

To calculate the tilt degree, a mathematic plane is created for the upper panel and derived vectors, $\vec{v_1}$ and $\vec{v_2}$, on a plane to calculate the normal vector to the mathematic plane. A normal vector is obtained from the cross product of $\vec{v_1}$ and $\vec{v_2}$. Consequently, the tilt degree is obtained by utilizing the vertical direction unit vector, [0, 0, 1], and the normalized vector, $\vec{n}$.

$$\vec{v_1} = \vec{a_i} - \vec{b_j} \quad \vec{v_2} = \vec{b_j} - \vec{c_k} \tag{10}$$

$$\vec{n} = \frac{\vec{v_1} \times \vec{v_2}}{\left|\vec{v_1} \times \vec{v_2}\right|} \tag{11}$$

$$Tilt = cos^{-1}(\vec{n} \cdot [0, 0, 1]) \tag{12}$$

De-center and de-space are obtained by manipulating the position vectors of $\vec{a_i}$, $\vec{b_j}$, $\vec{c_k}$ and $\vec{d_l}$.

$$\text{De-center} = \sqrt{\left(\frac{a_{ix} + b_{jx} + c_{kx} + d_{lx}}{4}\right)^2 + \left(\frac{a_{iy} + b_{jy} + c_{ky} + d_{ly}}{4}\right)^2} \tag{13}$$

$$\text{De-space} = \left(\frac{a_{iz} + b_{jz} + c_{kz} + d_{lz}}{4}\right) \tag{14}$$

Conclusively, the maximum value of the degree of alignment obtained through the aforementioned process is presented in Table 3.

2.4 Experimental results of alignment errors

After manufacturing the deployable structure using conventional CNC machining, we measured the degree of alignment employing the 6-axis touch probing based CIMCORE ® ARM (Portable Measuring Arm), which has a resolution of 30 μm, as shown in Fig. 11. This is a contact type measurement device that is capable of measuring displacements in the global coordinate.

The measuring points on the lower panel (A_1, B_1, C_1) and upper panel (A_2, B_2, C_2) were fabricated 90mm to the radial direction from the center of each panel with an interval angle of 120 degrees, as shown

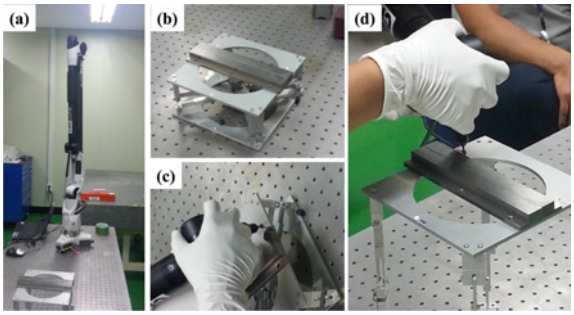

Fig. 11 Measurement probe (a) and scenes (b)~(d)

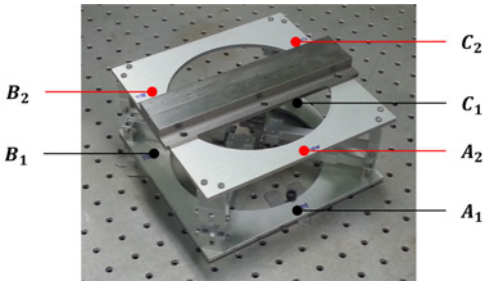

Fig. 12 The upper/lower panel measurement points

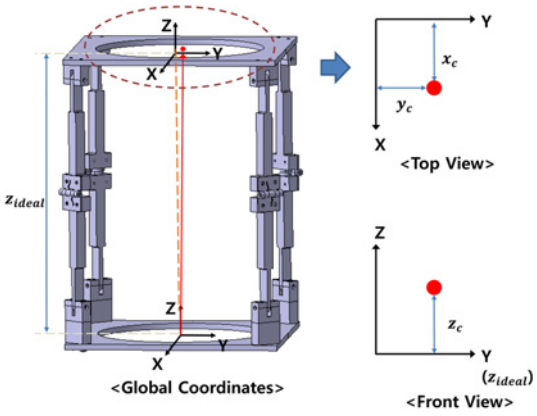

Fig. 13 Calculating de-center and de-space

in Fig. 12. We measured the displacements of the measuring points of the upper and lower panels repeatedly before and after deployment. Then, we produced two panels by using the averaged value of three times the measured displacements of the measuring points of the lower panel and the upper panel, respectively, and derived two circle equations that pass three points on each panel. Based on each center (x_c, y_c, z_c) of the two obtained circles in Fig. 13, de-center and de-space were calculated.

$$De\text{-}center = \sqrt{x_c^2 + y_c^2}, \quad De\text{-}space = z_c \tag{15}$$

For the tilt calculation, the two panels are defined, as shown in Fig. 14, as the ideal and real upper panels. Then, the tilted angles are calculated as follows:[13]

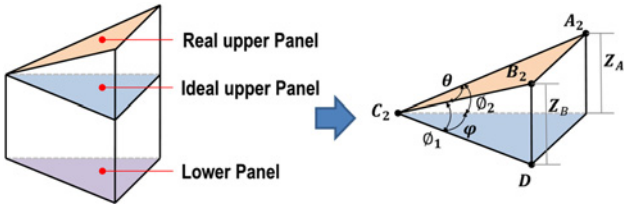

Fig. 14 Schematic diagram for the calculation of tilt

Table 4 Experimental results for the alignment error

Alignment Result	De-space (μm)	Tilt (μrad)	De-center (μm)
Average	180.2	218.8	617.5

$$\varnothing_1 = sin^{-1}\left(\frac{z_B}{B_2C_2}\right), \quad \varnothing_2 = sin^{-1}\left(\frac{z_A}{C_2A_2}\right) \tag{16}$$

We set the direction of $\overrightarrow{C_2D}$ as the x-axis of the global coordinate system. Therefore, the connection line between the measuring points on the upper panel can be calculated. Then, we can obtain the tilted angle of the top panel.

$$\begin{aligned}
&\overrightarrow{C_2B_2} = |C_2B_2|(cos\varnothing_1, 0, sin\varnothing_1)\\
&\overrightarrow{C_2A_2} = |C_2A_2|(cos\varnothing_2 cos\varphi, sin\varnothing_1 sin\varphi, sin\varnothing_2)\\
&\overrightarrow{C_2A_2}\cdot\overrightarrow{C_2B_2} = |C_2A_2||C_2B_2|(cos\varnothing_1 cos\varnothing_2 cos\varphi + sin\varnothing_1 sin\varnothing_2)\\
&\therefore \varphi = cos^{-1}\left(\frac{cos\theta - sin\varnothing_1 sin\varnothing_2}{cos\varnothing_1 cos\varnothing_2}\right)\\
&\left(where,\quad cos\theta = \frac{|C_2A_2|^2 + |C_2B_2|^2 - |A_2B_2|^2}{2|C_2A_2||C_2B_2|}\right)
\end{aligned} \tag{17}$$

$$\therefore \vec{n} = \frac{\overrightarrow{C_2A_2}\times\overrightarrow{C_2B_2}}{\left\|\overrightarrow{C_2A_2}\times\overrightarrow{C_2B_2}\right\|}, \quad \text{Tilt} = cos^{-1}(\vec{n}\cdot[0,0,1]) \tag{18}$$

Finally, the experimental results on the alignment error are presented in Table 4.

The difference between the experimental and the theoretical analysis results stem from the gravity effect and measurement method. In the theoretical analysis, we assume the mechanism is not under gravity, as in space. On the contrary, the experiment is carried out under gravity. For de-space, the experimental and the theoretical analysis results are very similar since the gravity in the experimental environment plays a role in preloading to the z-axis direction and causes the worst position of each joint's clearance to approximate the worst position in the theoretical analysis. The experimental results regarding tilt were much better than the theoretical results because the gravity pushed down all joints in the four supporting modules to the worst positions, resulting in the minor slope of the upper panel. For de-center, the experimental results were much higher than the theoretical results since we utilized a touch probing based measurement device (CIMCORE ® ARM) and caused the instability of the upper panel at the moment of contact.

3. Conclusions

In this paper, we designed a simple deployable mechanism for the optical structure of a small satellite. The deployable mechanism employed a passive driving mechanism powered by the restoring force of the spring hinge. In order to confirm the feasibility of the concept design, alignment errors were theoretically analyzed. Based on the theoretical results (a de-space of 180.0 μm, a tilt of 1941.3 μrad, and a de-center of 45.3 μm), the proposed mechanism was constructed. Then, the degree of alignment was measured employing the 6-axis touch probing based measurement device. As a result, the alignment errors were confirmed (a de-space of 180.2 μm, a tilt of 218.8 μrad, and a de-center of 617.5 μm). Comparing to the required alignment specifications, except for de-space, alignment errors were relatively high with respect to realizing a 1-m ground resolution. In order to satisfy the target alignment, therefore, the following additional research will be carried out

- A customized displacement sensing system will be constructed to reduce the de-center error since the main de-center error originates from the movement of the upper panel due to the touching process during probing.
- A deployment test will be carried out in microgravity conditions mimicking a space environment.
- A parts fabrication manual and assembly manual will be provided to reduce the machining tolerance.
- A mechanism will be studied to reduce clearance at each joint.

ACKNOWLEDGEMENT

This work was supported by the Global Surveillance Research Center (GSRC) Program funded by the Defense Acquisition Program Administration (DAPA) and Agency for Defense Development (ADD).

REFERENCES

1. NASA, “NSAS FBC Task Final Report,” http://mars.nasa.gov/msp98/misc/fbctask.pdf (Accessed 23 OCT 2015)
2. eoProtal Directory, “GeoEye-1,” https://eoportal.org/web/eoportal/satellite-missions/g/geoeye-1 (Accessed 23 OCT 2015)
3. Harrison, F. A., Craig, W. W., Christensen, F. E., Hailey, C. J., Zhang, W. W., et al., “The Nuclear Spectroscopic Telescope Array (Nustar) High-Energy X-ray Mission,” The Astrophysical Journal, Vol. 770, No. 2, pp. 103, 2013.
4. Xu, Z., Guannan, Y., Hai, H., and Xinsheng, W., “Deployment Analysis and Test of a Coilable Mast for BUAA Student Micro-Satellite,” Proc. of IEEE 3rd International Symposium on Systems and Control in Aeronautics and Astronautics (ISSCAA), pp. 1329-1332, 2010.
5. eoProtal Directory, “DST (Dobson Space Telescope,” https://eoportal.org/web/eoportal/satellite-missions/d/dst (Accessed 21 OCT 2015)
6. Nakamura, Y., Eishima, T., Nagai, M., Funase, R., Enokuchi, A., et al., “University of Tokyo's Ongoing Student-Lead Pico-Satellite Projects-Cubesat Xi and Prism,” Proc. of 55th International Astronautical Congress, IAC-04-1AA-4.11.4.06, 2004.
7. Hachkowskil, M. R., “Mechanism Design Principles for Optical-Precision, Deployable Instruments,” Proc. of 41st Structures, Structural Dynamics, and Materials Conference and Exhibit, AIAA-2000-1409, 2000.
8. Telescope-Optics, “5.3. Misalignment,” http://www.telescope-optics.net/induced2.htm (Accessed 21 OCT 2015)
9. Lee, S.-Y., Kim, G., Lee, Y.-S., and Kim, G.-H., “Optical Design and Tolerance Analysis of a New Off-Axis Infrared Collimator,” Int. J. Precis. Eng. Manuf., Vol. 15, No. 9, pp. 1883-1888, 2014.
10. Angelidis, A. and Vosniakos, G.-C., “Prediction and Compensation of Relative Position Error Along Industrial Robot End-Effector Paths,” Int. J. Precis. Eng. Manuf., Vol. 15, No. 1, pp. 63-73, 2014.
11. Akhadkar, C. A., Deoghare, A. B., and Vaidya, A. M., “Influence of Joint Clearance on Kinematic and Dynamic Parameters of Mechanism,” IOSR Journal of Mechanical and Civil Engineering, Vol. 10, No. 6, pp. 39-52, 2014.
12. Schwab, A. L., Meijaard, J. P., and Meijers, P., “A Comparison of Revolute Joint Clearance Models in the Dynamic Analysis of Rigid and Elastic Mechanical Systems,” Mechanism and machine theory, Vol. 37, No. 9, pp. 895-913, 2002.
13. £uczak, S., “Guidelines for Tilt Measurements Realized by Mems Accelerometers,” Int. J. Precis. Eng. Manuf., Vol. 15, No. 3, pp. 489-496, 2014.